

https://dspace.org/

Relationships Between StressResponsive Biomarkers ART Adherence and Viral Suppression Among Adolescent Girls and Young Women Living With HIV in South Africa An HPTN 068 Analysis

M C D Stoner; N K Kelly; Francesc Gomez-Olive Casas; Kathleen Kahn; D Wagner ...

https://hdl.handle.net/10539/39306
WOS

Downloaded from a DSpace repository. https://dspace.org/

Laser shock peening of laser powder bed fusion produced Ti6Al4V for potential improvements to implant performance

Tristan Strydom[1*], *Claudia* Polese[1,2], and *Daniel* Glaser[3,4]

[1]School of Mechanical, Industrial and Aeronautical Engineering, University of the Witwatersrand, 2000 Johannesburg, South Africa
[2]DSI-NRF Centre of Excellence in Strong Materials, hosted by the University of the Witwatersrand
[3]Council for Scientific and Industrial Research (CSIR), National Laser Centre, 0081 Pretoria, South Africa
[4]Mechanical Engineering, Nelson Mandela University, 6019 Gqeberha, South Africa

Abstract. Titanium alloy based implants are becoming more common with medical advancements and longer global life expectancy. With its geometrical design freedom, low material wastage, and mass customisation, additive manufacturing has found growing use in biomedical applications. In this study, laser shock peening without coating (LSPwC) was investigated as a means to enhance the surface and mechanical properties of selective laser melted Ti6Al4V implants. The application of LSPwC was found to induce a favourable surface oxide layer, increase the measured surface roughness and hardness, and reverse the tensile residual stresses imparting deep, high-magnitude compressive residual stresses. The combination of oxide layer, increased roughness, and induced compressive stress will potentially improve implant osseointegration and increase fatigue life.

1 Introduction

Biomedical implants have become commonplace with advances in modern medical technology, not only in cases of severe injury or disease but also as quality-of-life investments. The use of implants is set to continue rising with increased global life expectancy and younger patients receiving orthopaedic treatments, such as knee or hip replacements. Orthopaedic implants are often made of titanium (Ti) alloys, especially at the bone-implant interface. Ti6Al4V is the most common alloy used in implants due to the favourable combination of high strength to weight, excellent corrosion resistance, and biocompatibility [1]. Ti6Al4V components, however, can be challenging to manufacture with conventional methods, especially with complex geometries, due to work hardening and the high costs involved.

Laser-based powder bed fusion of metals (PBF-LB/M or LPBF) is an additive manufacturing process that uses a high-power laser to selectively melt and fuse metal powders layer-wise to create near-fully dense components [2]. It has seen a rise in interest in

* Corresponding author: triststrydom@gmail.com

© The Authors, published by EDP Sciences. This is an open access article distributed under the terms of the Creative Commons Attribution License 4.0 (https://creativecommons.org/licenses/by/4.0/).

the biomedical field as it can effectively fabricate Ti6Al4V parts with near-limitless geometric freedom, allowing for optimised patient-specific designs with reduced cost and time [3, 4]. Furthermore, the parts can have controlled porosity and lattice-formed structures that can tailor the material properties of LPBF Ti6Al4V to better mimic bone, reducing stress-shielding (i.e. rigidity mismatch between implant and bone) [5] and can have functionally graded surfaces and features which can increase osseointegration (i.e. the integration of human bone cells to the surface of implants) [4, 6].

While the advantages of LPBF-produced parts are clear, there are significant drawbacks. Numerous studies on the properties of Ti6Al4V produced by LPBF noted high tensile residual stresses (TRS), poor ductility, and surface and sub-surface pore formation due to the large thermal gradients and layer-wise forming [7, 8]. These TRS drastically reduce fatigue life, can initiate cracking in LPBF parts, and in combination with pores, reduce corrosion resistance. For implants, where complex fatigue loadings and corrosive environments (physiological fluids and enzymes) are typical, these can be significantly detrimental.

As-built LPBF parts are often stress relieved post manufacture with treatments such as Hot Isostatic Pressing (HIP), annealing, or aging to remove the TRS, improve ductility, alter the microstructure, remove anisotropy and close pores [9], or with in-situ preheating in attempts to reduce TRS and anisotropy [10]. Despite the ability to remove the TRS and offer improvements to fatigue life, these processes cannot induce compressive residual stresses (CRS), which significantly increase fatigue life, nor fully close sub-surface or surface pores. Additionally, post-processing to improve the surface conditions of LPBF implants is commonly needed to enhance bone cell adhesion and proliferation and promote osseointegration [11, 12].

Laser shock peening (LSP) is a post-processing technique that modifies the surface and near-surface of a material through thermal, mechanical, and chemical interactions at the laser-material interface. The basic LSP interaction is illustrated in **Fig. 1.** A high-power laser impacts the material surface in short-pulse bursts, forming high-pressure plasma-induced shock waves that propagate into the material when confined by the water overlay. The effect is the plastic deformation of the material, inducing deep, high-magnitude CRS, which increases resistance to surface-related failures, such as fatigue and stress corrosion cracking [13]. Furthermore, LSP increases hardness, refines the grain structure, and increases strain hardening at the surface, which serve to retard crack growth, thereby increasing the lifespan of the material, as shown in numerous studies on Ti-alloys [14–16].

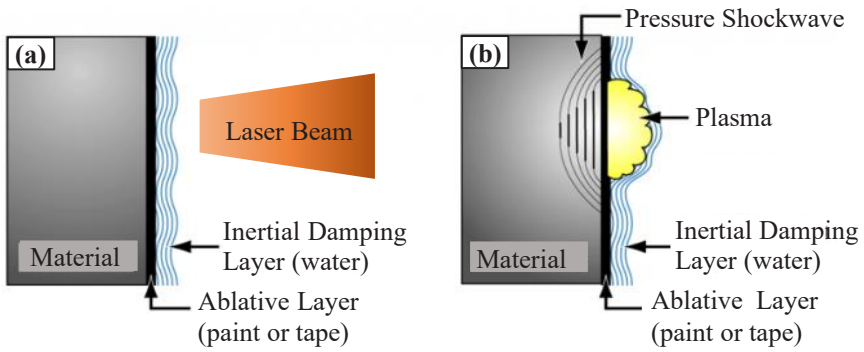


Fig. 1. LSP process (a) before laser impact, (b) after laser impact; images adapted from [45].

LSP is a parameter-dependent process where variation in the CRS magnitude and depth of penetration can be achieved by varying the coverage or pulse (or spot) density, application pattern, laser power intensity, pulse duration, and spot size [17]. Additionally, LSP can be conducted without the use of the protective or ablative coating (LSPwC), allowing direct

laser-material interaction causing significant changes at the material surface, including increased roughness and oxide formations [18, 19].

The changes induced by LSPwC may prove beneficial to the surface of implants. Studies have shown that surface topography has a significant influence on the bone formation rate [20], where variations in surface texture can affect the cellular response at an implant surface and that an increase in surface roughness is positively correlated with improved bone-implant interface [21]. Roughness at the surface greater than 2 µm has shown better bone interface [22], and implant surfaces with Ra values of 3-5 µm show better osteoblast adhesion in vivo and in vitro [23]. Additionally, a TiO_2 oxide layer has also been shown to increase cell growth on the implant surface and acts as an antibacterial layer [12, 23, 24]. For example, a study concluded that thermal oxidation and increased roughness at the surface "allows the colonisation and activities of bone-lineage cells" [25].

LSP may be an attractive method to counteract the TRS inherent in LPBF parts while imparting beneficial surface modifications that can increase implant osseointegration. Previous studies have examined LSP as a means of tailoring the RS of LPBF parts, for example in [26]. There is scope to examine the effects of LSPwC on as-built LPBF Ti6Al4V as a surface modification technique to improve osseointegration and increase fatigue life. The focus of the study is therefore to investigate the use of LSPwC as a post-processing technique to mitigate some of the negative features of LPBF Ti6Al4V and to potentially enhance properties of an LPBF Ti6Al4V implant surface to promote better osseointegration. Investigations included qualitative microscopy of the surface and microstructure, surface roughness and hardness evaluations, and residual stress characterisation.

2 Materials and methods

2.1 AM samples

All samples investigated in this study were built using an SLM 125 machine (SLM Solutions, Germany) equipped with a single 400 W IPG fibre laser at Metal Heart (Gauteng, South Africa). Atomised Ti6Al4V powder and recommended printing parameters provided by SLM Solutions were used.

The samples were built directly onto the substrate as rectangular prisms with nominal dimensions of 20 x 20 x 6 mm with a layer thickness of 30 µm in three orientations, 0, 45, and 90 degrees relative to the base plate, as illustrated in **Fig. 2**. These orientations will be referred to as "flat", "angled", and "vertical" samples, respectively. The flat samples were a single batch, and the angled and vertical samples were another. In total, 48 samples were built, with 16 samples per build orientation.

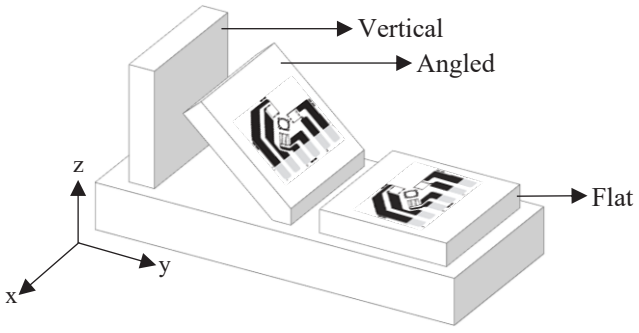


Fig. 2. Illustration of the sample build orientations, with strain gauge rosette placement to highlight relevant faces investigated.

The samples did not undergo stress relieving or post processing and were left "as-built". They were removed from the substrate via wire electrical discharge machining (WEDM) prior to further testing and processing. No significant part distortion was observed in the samples, as expected for the relatively small scale of the samples; however, building directly onto the base plate did influence the stress state of the flat samples.

The portion of the samples investigated further was the major surface area, i.e. the 20 x 20 mm "front" (zx) or "top-facing" (xy) surface (illustrated by the strain gauge placement in **Fig. 2**), in addition to a cross-sectional 20 x 6 mm face. The sample surfaces were prepared as required for the relevant testing and measurement techniques.

2.2 Methods

2.2.1 LSP processing

The samples were processed at the Council for Scientific and Industrial Research National Laser Centre (CSIR NLC) in South Africa, using an in-house developed processing platform incorporating a Quanta-Ray Pro series Nd:YAG pulsed nanosecond laser (Spectra-Physics, United States). The laser operates at a 1064 nm wavelength with a pulse duration of 8.6 ns and a frequency of 20 Hz. The samples were peened with a power intensity (PI) of 10 GW/cm^2 and a spot diameter (D) of 0.8 mm. The spot density, or spots per mm^2 (N_p), was varied with N_p = 5, 10, 20, and 40 spots/mm^2 to assess the efficacy of LSP on the as-built LPBF Ti6Al4V. An approximate 10x10 mm area was peened at the centre of the samples. All samples were processed without using an ablative protective coating, i.e. LSPwC.

The parameters chosen were based on existing literature for peening wrought Ti6Al4V, which suggests PI greater than 5 GW/cm^2, typically in the 8 – 10 GW/cm^2 range [13]. Research conducted within Wits University on Ti6Al4V, as done by Glaser et al. [27], using a PI of 10 GW/cm^2, a D of 0.8 mm, and a N_p = 40 found favourable outcomes of LSPwC on LPBF Ti6Al4V at this parameter set.

LSP coverage is achieved using a typical raster pattern, as shown in **Fig. 3** (a), where the laser is scanned left-to-right and vice versa in the x-direction, with steps in the y-direction. The spot overlap, and thereby the spot density, is controlled by varying the scan speed in the x-direction and step distance in the y-direction. An illustration of a high and low spot density is shown in **Fig. 3** (b) and (c).

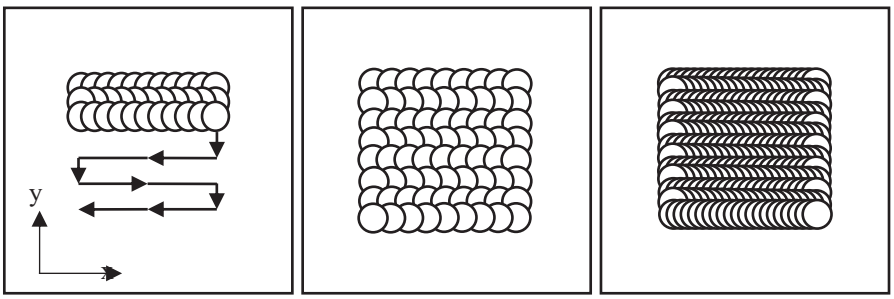


Fig. 3. (a) Typical LSP raster pattern with scan in x-direction and steps in y-direction, (b) Low N_p, and (c) High N_p.

2.2.2 Microscopy

Low-magnification Optical Light Microscopy (OLM) and high-magnification Scanning Electron Microscopy (SEM) techniques were used to characterise the as-built and peened material's surface topography, morphology, and microstructure. For microstructural analyses, the samples were polished to a mirror finish according to metallographic standards for Ti6Al4V and were then etched with Kroll's reagent. Imaging of the microstructure was conducted at the major face and a cross-section through the samples.

OLM was conducted using an SMZ1500 (Nikon Corporation, Japan) and a BA310Met (Motic, Hong Kong). SEM was performed on the Sigma 300 (ZEISS, Germany) and the Vega 3 (TESCAN, Czech Republic). The surface imaging allowed for the comparison and interpretation of the effects of the LSPwC on the as-built material. Energy Dispersive Spectroscopy (EDS) characterised the oxide formation at the peened surface.

2.2.3 Roughness

Surface roughness, R_a, was assessed using an SRT62-10 (HUATEC, China) contact probe inductance profilometer. The cut-off length, λ_c, was 2.5 mm, and the measurement range was 4L and 2L within the as-built and peened areas, respectively. Three repeated measurements at five points over the surface, in both the "x" and "y" direction, were taken to calculate a mean R_a value for each sample, and orientation.

2.2.4 Vickers hardness

Hardness testing was conducted using the Vickers method via a FALCON 500 (InnovaTest, Netherlands) automated hardness testing system at HV_{10}. Testing was performed according to ASTM E92 specifications [28]. Macroindentation at HV_{10} was used to find a mean hardness value at the major surface area, using 16 values per sample. To limit the inaccuracy of the hardness measurements, the sample surfaces were polished to a mirror finish per good practice guides and ASTM specifications.

2.2.5 Residual stress analysis - Incremental Hole Drilling

Residual stresses were assessed using the Incremental Hole Drilling (IHD) method, according to the ASTM E837-13a [29] standard. The process used the MTS3000-Restan IHD machine and associated Restan stress measurement and EVAL software (SINT Technology, Italy). The drilling was done with FG-38 cone mill bits (Wright Millners, South Africa) with a nominal diameter of 1.8 mm. Eighty (80) steps were drilled at increments of 0.015 mm up to a total depth of 1.2 mm. Lower step increments result in reduced thermal effects and, thus, more accurate measurements [30], which is useful in samples with non-uniform stress distributions. The CEA-06-062UL-120 tri-axial ASTM Type-A strain gauges (Micro-Measurements, United States) were used to obtain the strain readings. The gauges were placed at the centre of the sample or peened area such that the residual stresses were measured in the x- and y-directions or x- and z-directions (see **Fig. 2**). The gauge was connected to a QuantumX 440B (HBM) data acquisition system. Results were processed using the Restan EVAL 7.2 Premium evaluation software, where the ASTM E837-13a non-uniform method with 20 linear steps was used, and Tikhonov correction was applied. A Young's modulus of 113 GPa and 117 GPa is reported [31] for Ti6Al4V parts produced on the SLM 125 in the horizontal and vertical direction, respectively. A value of 115 GPa was chosen as the mean of this value. The Poisson's ratio used is 0.3. The values were based on existing literature.

Sample preparation and gauge adhesion would follow the instructions and recommendations of references [29, 30, 32].

3 Results and discussions

3.1 Surface texture and microstructure

The as-built LPBF surface of a flat sample in (a) and a vertical sample in (b) are shown in **Fig. 4**, where visible surface features include melt lines, overlaps, balling, partially fused surface particulate and powder, which were seen across all samples and is consistent with existing literature [33, 34].

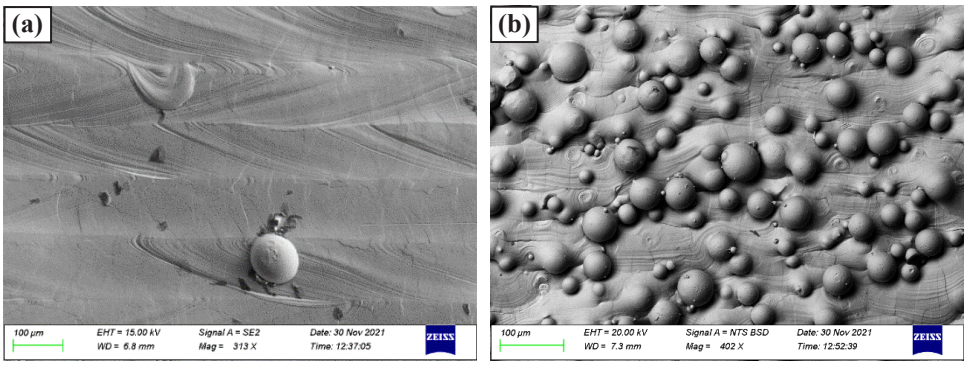


Fig. 4. Electron imaging of the as-built surfaces of the (a) flat sample and (b) vertical sample, showing typical features of the SLM process such as scan lines, balling, and spherical particulate.

LSPwC is a thermo-mechanical process where the absence of protective coating allows direct thermal, chemical, and mechanical changes at the material surface [18, 19]. The surface state is altered through molten material flow, splatter, and the formation of an oxide layer. The general effects of LSPwC are well illustrated in **Fig. 5**, which shows the boundary of the peened area (left-hand side) at the surface of a flat LPBF sample. It is evident how the surface has been melted, splatter (white dots) has been formed, and features of the as-built surface are no longer visible.

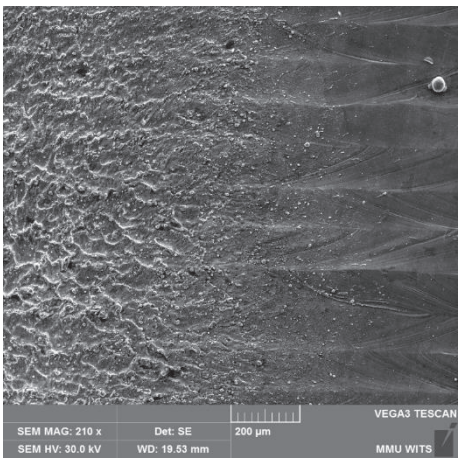


Fig. 5. Boundary of peened area on flat sample, illustrating the effects of LSPwC treatment, at Np = 40, on the material surface including molten flow and splatter.

The peened surfaces presented visible laser impact craters and the formation of an oxide layer. The difference between the visible surface state at the lowest and highest spot density, $N_p = 5$ and $N_p = 40$, is illustrated in **Fig. 6** showing the oxide layer (black coating) and the impact craters (visible in (a)).

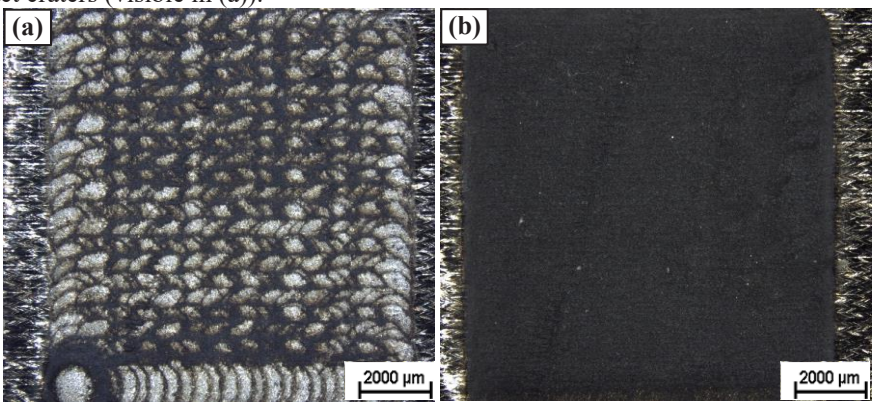


Fig. 6. Peened surface of two flat samples LSPwC treated at (a) $N_p = 5$ and (b) $N_p = 40$.

The build orientation of the samples did not have an observable effect on the surface deformations or oxide formation, specifically at higher N_p values which presented with similar macro-phenomena. The general surface appearance of the samples peened at $N_p = 10$ and $N_p = 20$ was closer to **Fig. 6** (b) than that of **Fig. 6** (a). During SEM imaging, EDS was utilised to characterise the oxide layer formation. The results in **Table 1** show that the oxide is likely a heterogenous layer of TiO_2 and Al_2O_3, although small quantities of TiO likely exist.

Table 1: EDS spectrum results (TESCAN VEGA3).

Element	Atomic No.	Series	unn. C [wt.%]	norm. C [wt.%]	Atom C [at.%]	Compound	Comp. C [wt.%]
C	6.00	K	0.00	0.00	0.00		
O	8.00	K	56.47	23.55	61.10		
Al	13.00	K	4.37	1.82	2.80	Al_2O_3	3.44
Ti	22.00	K	57.52	74.63	36.1	TiO_2	96.56
Total:			118.36	100.00	100.00		

Increasing the N_p increases the cumulative effects of the LSPwC and will increase the damage to the surface and increase the amount of oxide formed. Further surface alterations include increases in surface undulations, reduction in the appearance of the spherical particulate and unfused powder, and closure of surface pores, voids, and microcracks. A comparison of the surface peened at $N_p = 5$ and $N_p = 40$ is shown in **Fig. 7**.

Fig. 8 presents a side-by-side image of the microstructure of the zx-face of an as-built sample and a sample peened at $N_p = 40$. The microstructure observed in the as-built LPBF Ti6Al4V (**Fig. 8** (a) and (b)) consists of a fine acicular martensitic phase with long columnar grains that grow parallel to the build height, consistent with literature. Varying microstructural size and distribution is observed relative to the respective orientation of the observed face, as found in [33, 34].

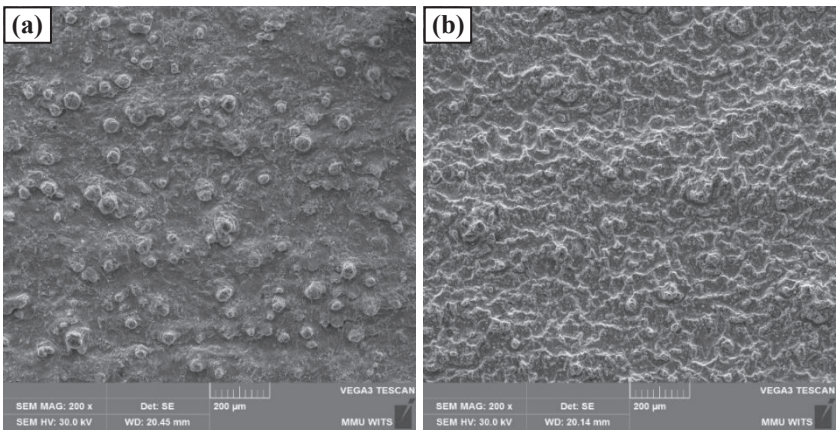


Fig. 8. Illustration of surface damage of two angled samples treated with LSPwC at (a) $N_p = 5$ and (b) $N_p = 40$.

The microstructure of samples treated with LSPwC at $N_p = 40$ is shown in **Fig. 8** (c) and (d). LSPwC, at all spot densities and for all build orientations, did not have any observable effect on the microstructure, at the surface or cross-sectional surface, in this study. LSP typically refines the grain structure introducing martensitic grains in Ti-alloys at the peened area, creating a gradient microstructure through the depth of the treated material [35]. In the case of LPBF-produced materials, which already possess a fine directional microstructure, it is difficult to assess the changes induced to the microstructure by LSPwC. No visible changes likely occurred at this scale; however, changes in the sub-grain scale likely occurred due to deformations induced by the LSP shockwaves, including an increase in dislocation densities[13, 35] which may present as an increase in hardness at the peened surface, as seen in [18].

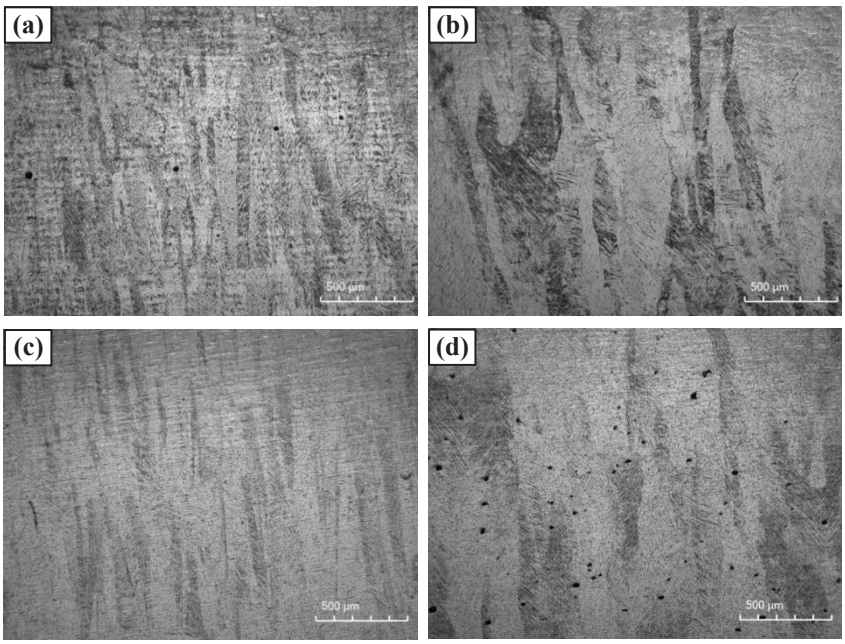


Fig. 7. Microstructure at a section of the major surface area for an as-built (a) angled and (b) vertical sample and of a (c) angled and (d) vertical sample peened with $N_p = 40$.

3.2 Surface roughness

Mean R_a values of measurements taken in two directions across the sample surface were used to calculate a total mean R_a for each sample set, which are visualised for comparison in **Fig. 9**. The as-built surfaces had mean roughness of R_a = 7.9±0.63 µm for the angled samples, whilst the vertical and flat sample orientations had values R_a = 6.2±0.38 µm and R_a = 4.3±0.36 µm, respectively. The maximum increase recorded for each orientation, with respect to the as-built state, was 41.31% to 6.1±0.37 µm for the flat samples treated at N_p = 40, 8.5% to 8.5±0.38 µm for the angled samples treated at N_p = 20, and 7.56% to 6.7±0.39 µm for the vertical samples treated at N_p = 5. A significant increase in the mean R_a is seen for the flat samples while a general trend of increasing roughness from the as-built state when LSPwC is applied is seen.

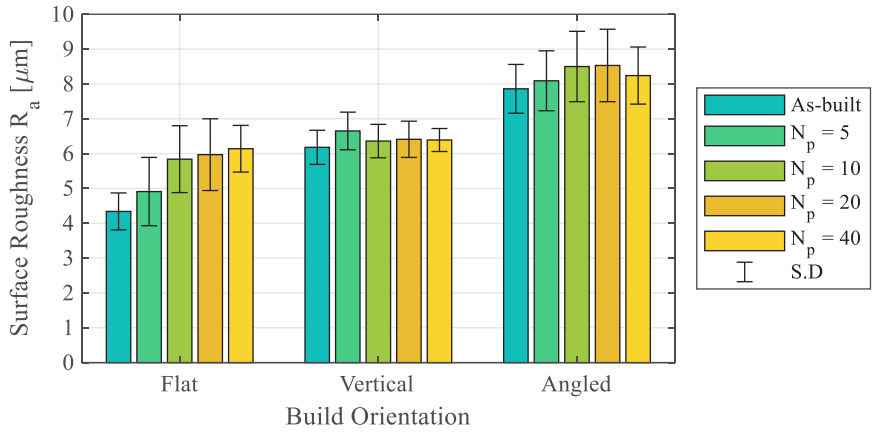


Fig. 9. Comparison of surface roughness, R_a, for the as-built material and the LSPwC treated material at the various N_p values for the respective build orientations.

The surface roughness of parts can significantly affect the performance and lifetime of the part and material. The effects of high surface roughness can be observed in decreased corrosion resistance where there is an increased area for corrosive agent ingress [36] and lowered fatigue life due to stress concentrators at the surface [37]. For implants, however, the increased surface roughness at the bone-implant interface can have a significant impact on the morphology of cells at the surface [25, 38, 39] and increase the degree and rate of bone adhesion. The surface roughness in this study showed an increase in the roughness within the range of values typically seen as beneficial to implants (R_a = 2–100 µm). Additionally, the SEM images indicated the presence of micro- and nanotopography and the formation of an oxide layer at the surface. This increased roughness, in conjunction with the presence of the oxide layer, will likely result in greater osseointegration at the treated surface.

3.3 Hardness

The respective calculated mean HV_{10} values, and associated errors, are visualised in **Fig. 10** for comparison. The as-built samples had an average measured HV_{10} surface hardness of 418.2±5.8, 338.2±6.3, and 334.6±6.1 for the flat, angled, and vertical orientations, respectively. For the flat and vertical samples, the increase in hardness continues from N_p = 5 to N_p = 20, where the mean hardness at N_p = 20 is 456.0±5.6 and 405.6±6.1, for the samples respectively. At N_p = 40, a minor decrease is observed for these samples. The angled samples had increasing hardness with spot density up to a maximum of 426.2±6.1 at N_p = 40. Significant increases in the mean hardness is observed with the application of LSPwC.

Further, an increase in N_p generally correlates to increased HV_{10} hardness at the surface. An apparent saturation point appears at $N_p = 20$ for the measured data for the flat and vertical samples. A decrease in measured hardness was observed for these orientations from $N_p = 20$ to $N_p = 40$. This may not indicate a global trend for LPBF Ti6Al4V when peened with the parameters used in this research, and more data is needed to draw a definitive conclusion.

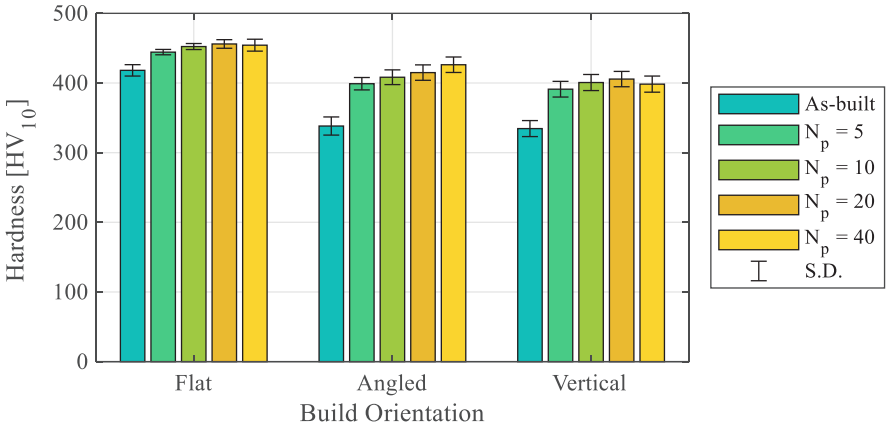


Fig. 10. Comparison of the Vickers hardness, HV_{10}, for the as-built material and the LSPwC treated material at the various N_p values, for the respective build orientations.

Although no microstructural changes were observed, the increased hardness indicates changes in the material at a sub-grain scale. The changes likely include increased dislocation density within the material and increased compressive strains within the material, limiting the deformation of the Vickers indenter [40]. Increased hardness can be attributed to the plastic deformation, strain hardening, and increased dislocation density caused by the peening process [35]. This increased hardness, while not directly related to osseointegration or biocompatibility, may create a material more resistant to corrosion or degradation within the body preventing the release of harmful ions and particulate into the body.

3.4 Residual stress

The IHD residual stress analysis results for the as-built and peened samples are presented in **Fig. 11**. The residual stress is plotted as the mean of the calculated principal stresses as a function of depth.

The as-built material in the current work exhibits large TRS for samples built in the angled and vertical build orientations, consistent with the literature [7, 8]. The flat samples, however, have low-magnitude compressive residual stresses (see **Fig. 11** (a)). A CRS state is not uncommon in LPBF parts and may be attributed to stress relaxation of the restrained material due to part removal from the substrate - this phenomenon is well visualised in the upward curling of thin LPBF-produced cantilevers, for example in [41].

Based on the calculated residual stress data for the as-built specimens, there appears correlation between increasing build orientation angle and increased residual stresses, with higher TRS found in the vertical samples. Assessing the residual stresses of as-built LPBF Ti6Al4V was not a core focus of this research, and further testing could examine the correlation between build orientation and residual stress. It is well established, however, that build orientation does influence the microstructure, anisotropy, and material properties of the

LPBF-built part. The as-built stresses were measured to assess the effect of LSPwC on the stress state.

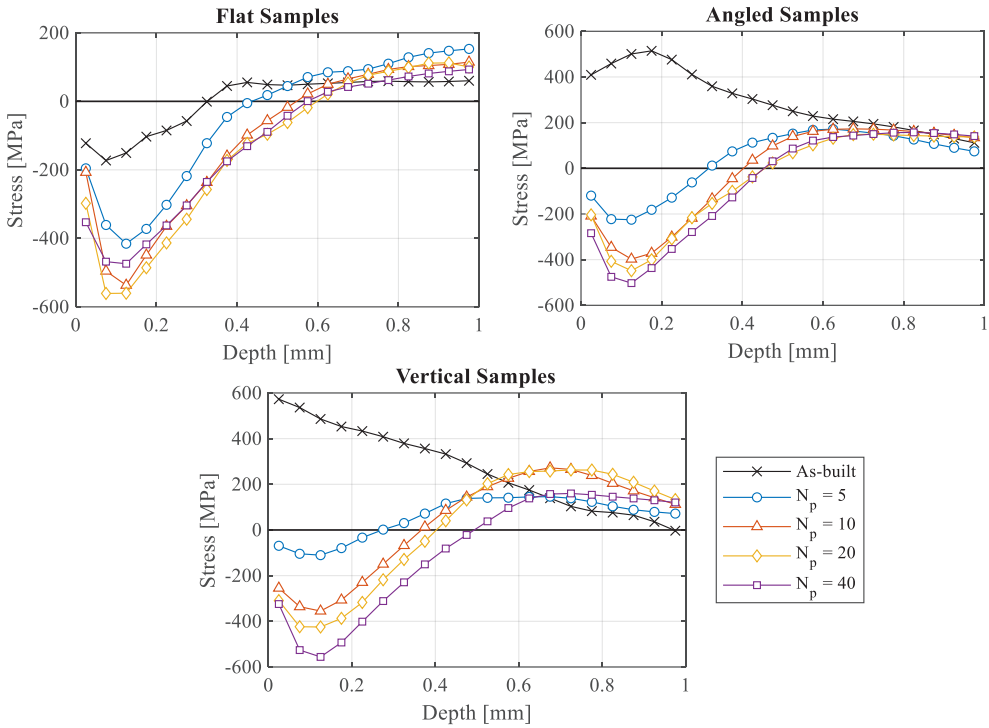


Fig. 11. Plots of the mean residual stress as a function of depth for the various sample build orientations in the as-built state and peened state at increasing N_p.

The application of LSPwC fully reverses the TRS state, inducing high-magnitude CRS fields that scale with magnitude and depth with an increase in the spot density N_p. In the case of the flat samples, the existing CRS state was enhanced with increased depth and magnitude. A typical increase of the compressive region in terms of depth across all samples was from between 0.2 and 0.3 mm at $N_p = 5$ to approximately 0.5 mm at $N_p = 40$. In the case of the flat samples, the CRS field depth is increased to 0.6 mm at $N_p = 40$. In addition, the LSPwC effectively reverses the TRS regardless of sample build orientation and associated as-built surface or residual stress state. The maximum CRS achieved for all orientations is similar, approaching a mean value of -600 MPa. These changes to the stress state will likely increase the fatigue resistance and life of LPBF Ti6Al4V components. Furthermore, the surface CRS in conjunction with the increased hardness and resurfacing would likely increase the corrosion resistance of parts.

A sequentially smaller increase in CRS field depth and magnitude is seen with increasing N_p. A significant increase in compressive residual stress is seen at $N_p = 5$, with smaller increases at $N_p = 10$, 20, and 40. In the case of the flat samples, a decrease in the magnitude of the CRS field is observed at $N_p = 40$ however, the depth remained constant. Similar findings were observed by Glaser et al. [44], showing that increasing spot coverage increases the depth and magnitude of CRS; however, a saturation point is reached where further coverage leads to diminishing returns. A balance between processing time, cost, and the desired stress field should be found within application parameters. For implant applications, an ideal value may be $N_p = 20$, which achieves high magnitude CRS and increases surface roughness in the desirable range.

It is possible that the CRS induced would have greater depth and magnitude if the specimens were stress-relieved and machined. Glaser et al. [27] found deeper CRS, at ca. 0.75 mm, when LSPwC was conducted on stress relieved and machined LPBF Ti6Al4V. However, it was noted in that study that machining before LSPwC would necessitate re-machining to remove the surface roughness induced by LSPwC. From the current research results, which show LSPwC induced CRS effectively in the as-built state, it appears viable to treat with LSPwC before machining to final dimensions.

4 Conclusions

This work explored the use of LSPwC on LPBF Ti6Al4V parts as a potential means to increase the material's performance in the context of medical implants. The objective was to assess the efficacy of LSPwC to improve the surface and material properties and compare them to the as-built LPBF Ti6Al4V. The surface state and residual stress profiles were investigated in the as-built and peened state and comparatively analysed.

Within the-context of this work, the following can be concluded on the effects of LSPwC on LPBF Ti6Al4V in the as-fabricated state:

- LSPwC induced morphological and topographical changes at the surface through ablated material splatter and flow, increasing the visible surface undulations and removing artefacts of the as-built LPBF surface.
- LSPwC induced a surface oxide layer comprised of TiO_2 and Al_2O_3.
- LSPwC increased the hardness (HV_{10}) and roughness (R_a) at the peened surface. These generally increase with increasing N_p, although outliers exist.
- LSPwC reversed the TRS of the LPBF process at the near-surface region and introduced significant CRS fields, which is true at all N_p values.
- The increase in N_p corresponds to an increase in the depth and magnitude of the CRS field.
- The build orientation of the samples had no significant impact on the ability of the LSPwC to induce the CRS field.

The findings suggest that LSPwC would be viable to treat three-dimensional components, with surface faces built in multiple orientations, with consistent outcomes to surface modification and residual stress. Within the context of this study, the LSPwC treatment achieved the aim of reversing the inherent TRS of the LPBF process and introducing the compressive residual stress field.

An implant of LPBF Ti6Al4V treated with LSPwC would likely see increased osseointegration or bone adhesion at the bone-implant interface due to the increased roughness and oxide layer, and a likely increase in fatigue life due to the CRS field induced by the peeing. These effects would improve the performance of an LPBF Ti6Al4V implant.

The use of LSPwC may be well suited to small parts or implants of LPBF Ti6Al4V in the as-built state (like dental, screws, cranial, etc.) where the process will, when applied to all faces, result in reversed stresses and the introduction of a CRS field.
For applications requiring a smoother surface finish, the layer(s) of material containing the undulations can be machined off while maintaining the integrity of the induced CRS fields in the material below.

Whilst the viability of LSPwC on LPBF Ti6Al4V is promising, more work can be done to assess the quality of the outcomes. Further work can be done on identifying the LSP parameter set for LPBF Ti6Al4V, possibly using LPBF-produced Almen strips. This could include testing the parts individually and in a combination of as-built (material and surface state), machined, and stress-relieved parts in combinations of the states. Future fatigue testing

of LPBF parts treated with LSPwC on the as-built surface with and without machining could include the stress-relieved and as-built state.

The authors would like to acknowledge the Collaborative Programme in Additive Manufacturing (CPAM) (Contract No.: CSIR-NLC-CPAM-21-MOA-WITS-01) and the DSI-NRF Centre of Excellence in Strong Materials – Strong Metallic Alloys Focus Area for financial support, and the DSI CSIR Rental Pool Program (Contract No.: NLC-LREQA22-CON-001) for the LSP processing.

References

1. F. H. (Sam) Froes, Titanium for medical and dental applications—An introduction. *Titanium in Medical and Dental Applications* (Elsevier, 2018), pp. 3–21. https://doi.org/10.1016/B978-0-12-812456-7.00001-9.
2. ASTM International, Additive manufacturing — Design — Part 1: Laser-based powder bed fusion of metals, ISO/ASTM 52911-1:2019(E), (2019).
3. J. M. Haglin, A. E. M. Eltorai, J. A. Gil et al., Patient-Specific Orthopaedic Implants, Orthop Surg, **8**, 417–424, (2016). https://doi.org/10.1111/os.12282.
4. P. Ahangar, M. E. Cooke, M. H. Weber et al., Current Biomedical Applications of 3D Printing and Additive Manufacturing, Applied Sciences, **9**, 1713, (2019). https://doi.org/10.3390/app9081713.
5. T. Takizawa, N. Nakayama, H. Haniu et al., Titanium Fiber Plates for Bone Tissue Repair, Advanced Materials, **30**, 1703608, (2018). https://doi.org/10.1002/adma.201703608.
6. X. P. Tan, Y. J. Tan, C. S. L. Chow et al., Metallic powder-bed based 3D printing of cellular scaffolds for orthopaedic implants: A state-of-the-art review on manufacturing, topological design, mechanical properties and biocompatibility, Materials Science and Engineering C, **76**, (2017). https://doi.org/10.1016/j.msec.2017.02.094.
7. P. Mercelis, & J. Kruth, Residual stresses in selective laser sintering and selective laser melting, Rapid Prototyp J, **12**, 254–265, (2006). https://doi.org/10.1108/13552540610707013.
8. J. L. Bartlett, & X. Li, An overview of residual stresses in metal powder bed fusion, Addit Manuf, **27**, 131–149, (2019). https://doi.org/10.1016/j.addma.2019.02.020.
9. S. A. Etesami, B. Fotovvati, & E. Asadi, Heat treatment of Ti-6Al-4V alloy manufactured by laser-based powder-bed fusion: Process, microstructures, and mechanical properties correlations, J Alloys Compd, **895**, 162618, (2022). https://doi.org/10.1016/j.jallcom.2021.162618.
10. B. Vrancken, S. Buls, J.-P. Kruth et al., Preheating of Selective Laser Melted Ti6Al4V: Microstructure and Mechanical Properties. *Proceedings of the 13th World Conference on Titanium* (Hoboken, NJ, USA: John Wiley & Sons, Inc., 2016), pp. 1269–1277. https://doi.org/10.1002/9781119296126.ch215.
11. T. Hanawa, Titanium–Tissue Interface Reaction and Its Control With Surface Treatment, Front Bioeng Biotechnol, **7**, (2019). https://doi.org/10.3389/fbioe.2019.00170.
12. T. Hanawa, 2.1 - Transition of surface modification of titanium for medical and dental use. In F.H. Froes, & M. Qian,eds., *Titanium in Medical and Dental Applications* (Woodhead Publishing, 2018), pp. 95–113. https://doi.org/https://doi.org/10.1016/B978-0-12-812456-7.00005-6.

13. K. Ding, & L. Ye, Physical and mechanical mechanisms of laser shock peening. *Laser Shock Peening* (Elsevier, 2006), pp. 7–46. https://doi.org/10.1533/9781845691097.7.
14. R. Sonntag, J. Reinders, J. Gibmeier et al., Fatigue performance of medical Ti6Al4V alloy after mechanical surface treatments, PLoS One, **10**, 1–15, (2015). https://doi.org/10.1371/journal.pone.0121963.
15. E. Wycisk, S. Siddique, D. Herzog et al., Fatigue Performance of Laser Additive Manufactured Ti–6Al–4V in Very High Cycle Fatigue Regime up to 109 Cycles, Front Mater, **2**, 2–9, (2015). https://doi.org/10.3389/fmats.2015.00072.
16. E. Maawad, Y. Sano, L. Wagner et al., Investigation of laser shock peening effects on residual stress state and fatigue performance of titanium alloys, Materials Science and Engineering A, **536**, 82–91, (2012). https://doi.org/10.1016/j.msea.2011.12.072.
17. Y. Sano, M. Obata, T. Kubo et al., Retardation of crack initiation and growth in austenitic stainless steels by laser peening without protective coating, Materials Science and Engineering: A, **417**, 334–340, (2006). https://doi.org/10.1016/j.msea.2005.11.017.
18. U. Trdan, J. A. Porro, J. L. Ocaña et al., Laser shock peening without absorbent coating (LSPwC) effect on 3D surface topography and mechanical properties of 6082-T651 Al alloy, Surf Coat Technol, **208**, 109–116, (2012). https://doi.org/10.1016/j.surfcoat.2012.08.048.
19. M. Rozmus-Górnikowska, Surface Modifications of a Ti6Al4V Alloy by a Laser Shock Processing, Acta Phys Pol A, **117**, 808–811, (2010). https://doi.org/10.12693/APhysPolA.117.808.
20. B. Boyan, Role of material surfaces in regulating bone and cartilage cell response, Biomaterials, **17**, 137–146, (1996). https://doi.org/10.1016/0142-9612(96)85758-9.
21. D. Buser, R. K. Schenk, S. Steinemann et al., Influence of surface characteristics on bone integration of titanium implants. A histomorphometric study in miniature pigs, J Biomed Mater Res, **25**, 889–902, (1991). https://doi.org/https://doi.org/10.1002/jbm.820250708.
22. A. Wennerberg, C. Hallgren, C. Johansson et al., A histomorphometric evaluation of screw-shaped implants each prepared with two surface roughnesses, Clin Oral Implants Res, **9**, 11–19, (1998). https://doi.org/10.1034/j.1600-0501.1998.090102.x.
23. A. N. Aufa, M. Z. Hassan, & Z. Ismail, Recent advances in Ti-6Al-4V additively manufactured by selective laser melting for biomedical implants: Prospect development, J Alloys Compd, **896**, 163072, (2022). https://doi.org/10.1016/j.jallcom.2021.163072.
24. G. Wang, J. Li, K. Lv et al., Surface thermal oxidation on titanium implants to enhance osteogenic activity and in vivo osseointegration, Sci Rep, **6**, 1–13, (2016). https://doi.org/10.1038/srep31769.
25. L. Crespo, M. Hierro-Oliva, S. Barriuso et al., On the interactions of human bone cells with Ti6Al4V thermally oxidized by means of laser shock processing, Biomedical Materials, **11**, 015009, (2016). https://doi.org/10.1088/1748-6041/11/1/015009.
26. N. Kalentics, E. Boillat, P. Peyre et al., Tailoring residual stress profile of Selective Laser Melted parts by Laser Shock Peening, Addit Manuf, **16**, 90–97, (2017). https://doi.org/10.1016/j.addma.2017.05.008.
27. D. Glaser, S. N. Van Staden, N. Ivanovic et al., The Potential Enhancement of Components Produced by Metal Additive Manufacturing using Laser Shock

Processing. *18th Annual International RAPDASA Conference* (Durban, South Africa, 2017), pp. 85–99.
28. ASTM International, Standard Test Methods for Vickers Hardness and Knoop Hardness of Metallic Materials, ASTM E92-17, (2017). https://doi.org/10.1520/E0092-17.
29. ASTM International, Standard Test Method for Determining Residual Stresses by the Hole-Drilling Strain-Gage Method, ASTM E837-13a, (2013). https://doi.org/10.1520/E0837-13A.
30. P. V. Grant, J. D. Lord, & P. S. Whitehead, The Measurement of Residual Stresses by the Incremental Hole Drilling Technique, Measurement Good Practice Guide No. 53, (2006).
31. SLM Solutions Group AG, *Ti-Alloy Ti6Al4V ELI Material Data Sheet* (Germany).
32. Micro-Measurements, Strain Gage Installations with M-Bond 200 Adhesive, Instruction Bulletin B-127, (2015).
33. M. Simonelli, Y. Y. Tse, & C. Tuck, Effect of the build orientation on the mechanical properties and fracture modes of SLM Ti-6Al-4V, Materials Science and Engineering A, **616**, 1–11, (2014). https://doi.org/10.1016/j.msea.2014.07.086.
34. L. Thijs, F. Verhaeghe, T. Craeghs et al., A study of the microstructural evolution during selective laser melting of Ti-6Al-4V, Acta Mater, **58**, 3303–3312, (2010). https://doi.org/10.1016/j.actamat.2010.02.004.
35. L. Zhou, & W. He, *Gradient Microstructure in Laser Shock Peened Materials* (Springer Singapore, 2021). https://doi.org/10.1007/978-981-16-1747-8.
36. G. Chi, D. Yi, & H. Liu, Effect of roughness on electrochemical and pitting corrosion of Ti-6Al-4V alloy in 12 wt.% HCl solution at 35 °C, Journal of Materials Research and Technology, **9**, 1162–1174, (2020). https://doi.org/10.1016/J.JMRT.2019.11.044.
37. J. Schijve, *Fatigue of Structures and Materials*, **2nd** ed (Dordrecht: Springer Netherlands, 2009). https://doi.org/10.1007/978-1-4020-6808-9.
38. G. Matos, Surface Roughness of Dental Implant and Osseointegration, J Maxillofac Oral Surg, **20**, 1–4, (2021). https://doi.org/10.1007/s12663-020-01437-5.
39. M. Khandaker, S. Riahinezhad, F. Sultana et al., Peen treatment on a titanium implant: Effect of roughness, osteoblast cell functions, and bonding with bone cement, Int J Nanomedicine, **11**, 585–595, (2016). https://doi.org/10.2147/IJN.S89376.
40. K. Tosha, Influence of Residual Stresses on the Hardness Numberin the Affected Layer Produced by Shot Peening. *2nd Asia-Pacific Forum on Precision Surface Finishing and Deburring Technology* (Seoul, 2002), pp. 48–54.
41. I. Yadroitsava, S. Grewar, D. Hattingh et al., Residual Stress in SLM Ti6Al4V Alloy Specimens, Materials Science Forum, **828–829**, 305–310, (2015). https://doi.org/10.4028/www.scientific.net/MSF.828-829.305.
42. D. Glaser, C. Polese, A. M. Venter et al., Evaluation of laser shock peening process parameters incorporating Almen strip deflections, Surf Coat Technol, **434**, (2022). https://doi.org/10.1016/j.surfcoat.2022.128158.
43. Curtis-Wright Surface Technologies, Shot peening or laser peening: A comparative guide to their application(s), https://cwst.com/shot-peening-or-laser-peening/